A Novel Technique for Contrast Enhancement of Chest X-Ray Images Based on Bio-Inspired Meta-Heuristics

Jhilam Mukherjee, Bishwadeep Sikdar, Amlan Chakrabarti, Madhuchanda Kar and Sayan Das

Abstract Chest radiography is considered as one of the most important radiological tools in pulmonary disease diagnosis. Due to the generation of low contrast images of X-ray machines, the detection of the lesions is a difficult issue and prone to error for a radiologist. Hence, a contrast enhancement algorithm is an obvious choice to enhance the contrast of the image, thus increasing the accuracy of detection of the lesions. This paper not only proposes a new algorithm for contrast enhancement of digital chest X-ray images using particle swarm optimization (PSO), but it also introduces a benchmark dataset of digital chest radiographs to justify the supremacy of our proposed algorithm over that of state-of-the-art contrast enhancement algorithms.

Keywords Chest radiography · Contrast enhancement · PSO · Lung lesion Benchmarking database

J. Mukherjee (✉) · A. Chakrabarti
A.K. Choudhury School of Information Technology,
University of Calcutta, Kolkata, India
e-mail: jhilam.mukherjee20@gmail.com

A. Chakrabarti
e-mail: acakcs@caluniv.ac.in

B. Sikdar
Institute of Engineering Management, Kolkata, India
e-mail: rahulsikder223@gmail.com

M. Kar · S. Das
Peerless Hospitex Hospital, Kolkata, India
e-mail: madhuchandakar@yahoo.com

S. Das
e-mail: sadnayas@gmail.com

R. Chaki et al. (eds.), *Advanced Computing and Systems for Security*,
Advances in Intelligent Systems and Computing 666,
https://doi.org/10.1007/978-981-10-8180-4_5

1 Introduction

Lung cancer has become a serious health issue in recent days. Nearly 91% affected Indians are suffering death due to this disease [1]. The survival rate is increased if it is detected at an early stage. With the advancement of medical imaging technology, computer-aided diagnostic systems take a major role to predict this disease at an early stage. Although computed tomography (CT) images efficiently detect this disease at an early stage, this technology is not available throughout this country. Chest radiographs may become an alternative solution for this disease. Lung cancer is generally initiated by pulmonary nodules having a small white spot, visible in the lung parenchyma. Often these lesions are hindered by chest ribs. Besides, most of the X-ray scanners generate images that are of low contrast due to the presence of water in the human body, which makes interpretation of lesions a tedious job not only for a radiologist but also for a computer-aided diagnosis system. Although the increase in X-ray tube current can enhance the quality of the radiographs, it can also generate adverse effects on the human body. Hence, an appropriate contrast enhancement algorithm is required to enhance the image at a desired level.

In this paper, we have introduced a new chest X-ray dataset "Swash" for detection and prediction of malignancy in pulmonary nodules. Besides the dataset, we have also proposed a new methodology based on PSO for contrast enhancement of digital chest radiographs.

The rest of the paper is organized as follows: Sect. 2 discusses on the literature review in this domain. Algorithm and functions responsible for enhancement are illustrated in Sect. 4. Section 5 exhibits the result of this study. Finally, conclusions are drawn in Sect. 6.

2 Related Work

A digital medical image database was first introduced in digital mammograms known as digital database for screening mammography, which contains 2620 four-view screening digital mammograms [2]. A chest X-ray database of 247 scans of solitary pulmonary nodules has been proposed by Japanese Society of Radiological Technology (JSRT) [3]. Contrast enhancement increases the dynamic range of the image. There are many algorithms that can increase the contrast of an image to some extent. Histogram equalization (HE) [4] and linear contrast stretching (LCS) [5] are widely acceptable as they are very simple method to implement; however, these two are global contrast enhancement methods which have a tendency to incorporate noise in it. According to Chen and Ramli [6], HE increases the contrast using the middle value of the gray scale but not using the mean intensity value. This leads to a brightness

preservation problem of histogram equalization. The above-mentioned problems can be overcome by adaptive histogram equalization (AHE) technique where the intensity value is increased based on the local properties of the histogram [7]. In another modified algorithm of HE, fuzzy histogram is used to overcome the inconsistency present in the gray level of brightness preserving dynamic histogram preceded by a smoothing procedure using Gaussian kernel, and finally, the gray level value is increased dynamically. Based on clipping histogram equalization technique, a novel contrast enhancement method is proposed in [8], where a clipping histogram is performed by mean and the median value of the histogram intensity adaptively. Using a region-based image enhancement technique, the contrast of the radiographs has been [9] increased by selecting the seed point and then intensity is enhanced adaptively. Another novel contrast enhancement methodology has been sketched out in [10], where benchmark images and low contrast digital mammograms are enhanced using shearlet domain. Computing the local statistical value of the input images, adaptive histogram enhancement technique is proposed in [11] to increase the quality of radiographs. Based on the local bihistogram equalization technique, an adaptive contrast enhancement methodology has been sketched out [12] to enhance the contrast of the MRI images. Using genetic algorithm (GA), a novel contrast enhancement methodology has been proposed in [13] to enhance the contrast of natural source images as it has more dynamic range, and the authors claim that GA can increase it to some extent. Using particle swarm optimization (PSO) technique, a novel contrast enhancement methodology has been sketched out in [14].

3 Data Description

Our target dataset images are described in Sect. 3.1. Presently, 120 chest X-ray of Swash dataset are available on (http://www.cu-coe.in/samples/X-ray/Data.zip). All the images are collected from Peerless Hospital from March 2015 to November 2016 for those patients who come for their routine check for lung cancer diagnosis. While collecting the patient data, we have taken those data that are confirmed through biopsy or cytology test. The patient edge lies between 30–75 in both male and female patients. Among 120 patients, 77 patients are male and rest are female. In conventional X-ray imaging procedure, the X-ray beam passes through the human body to project the shadow of hard tissue to project as shadow on the film. This film is then processed and printed to get the picture of the organ. In this study, we have used CR type of digital X-ray images where a sensor is placed behind the patient instead of placing X-ray films in conventional radiography. This sensor is next attached to the computer to create the digital radiography.

3.1 Sample Size Calculation

The size of the sample can be calculated as

$$n = \frac{z^2 * se(1 - se)}{d^2 p} \tag{1}$$

At 95% confidence level, $z = 1.96$, Se is the sensitivity; here, we considered it as 80%. d is the precession 20%, and p is the prevalence considered as 10%. Hence, the sample size of the dataset is 307 (Figs. 1 and 2).

3.2 Description of the Chest X-Ray Images

- Size: A pulmonary nodule with size < 3 mm is clearly benign. However, all the pulmonary nodules larger than this specified size do not have same chances of malignancy.
  - A lung nodule with size ≤ 4 mm has 0% chance of malignancy.
  - A lung nodule with size ≤ 7 mm has 1% chance of malignancy.

Fig. 1 Chest radiographs with nodule

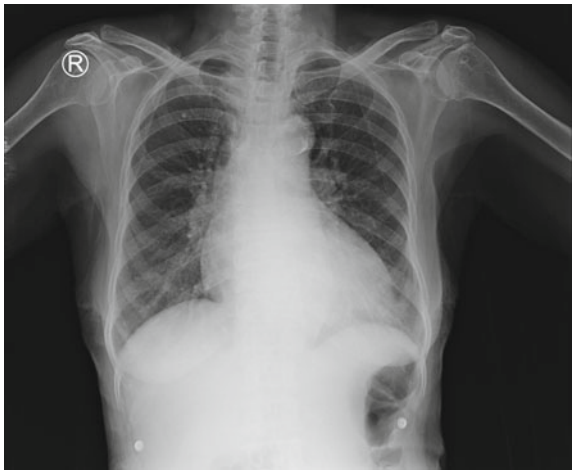

Fig. 2 Chest radiographs without nodule

  - A lung nodule with size $\leq$ 1 cm has 15% chance of malignancy.
  - A lung nodule with size $\leq$ 2 cm has 40% chance of malignancy.

- Shape: The shape of pulmonary nodule is categorized into six groups, namely round, oval, lobulated, speculated, irregular, and ragged. The pulmonary nodule with shape round, oval are benign and speculated, irregular and ragged are clearly malignant where as pulmonary nodules with shape lobulated is belongs to any group depending upon another features.
- Margin: The outline pulmonary nodule is categorized into four groups, namely smooth, lobulation, speculation, and irregular. The first two indicate benignity, and rest two are malignant.
- Presence and pattern of calcification: Calcification is a process in which calcium is deposited in living cell. If the nature of calcification of a nodule is either central or popcorn or laminated, it is a sign of benign lung nodule, whereas if its nature is speckled or eccentric, it is malignant one.
- State of Abnormality
  - Truly benign: The histopathology report clearly shows that it has no chances of cancer.
  - Probably benign: According to radiological features, the pulmonary nodules have very few chances of malignancy.
  - Probably malignant: According to radiological features, the pulmonary nodules have chances of malignancy.
  - Malignant: All the reports clearly reveal that it has cancer.
    Adenocarcinoma: This type of lung cancer generates due to abnormal growth of adeno cell of human body.
    Squamous cell carcinoma: This cancer arises due to abnormal growth of squamous cell.

  - Metastatic lung cancer: This type of cancer is generally initiated from other cancerous organs.

- Gender
- Position of the nodule: Human lung consists of five lobes. This confirm the localization of nodule on human lung.
- Coordinate position of the nodule:
- Types of Nodules

  Obvious
  Relatively Obvious
  Subtle
  Very Subtle
  Extremely Subtle

- Clinical Features

  Patient Age
  History of Malignancy
  Smoking History
  Hemoptysis

3.3 Annotation Process

In order to annotate the region of interest, we have designed a graphical user interface tool in MATLAB. Each radiologist marked on each subjects according to their expertise and visual interpretation considering a standard protocol of marking using this GUI tool through computer interface. All the radiologists mark on region of interest with a 5-mm interval on the boundary. This reduces inconsistency in marking. All the marks performed by each radiologist are stored in XML file along with slice number and its size. Each nodule candidate is assigned a unique identity number. They are assigned the number in increasing order from top left position to right bottom position. Each identification number remains the same in each slice in which it belongs. This procedure yields a single separate XML file for each subject.

3.4 Database Access Procedure

The original anonymized patient images in DICOM format along with its annotated image files of all subjects along with associated XML files and radiologists marked images of each patient have been uploaded to the following link (http://www.cu-coe.in/samples/X-ray/Data.zip) to download publicly and freely from the same link.

A registration procedure must be performed by each of the users before the sign-in process using users institutional email id. A unique password is automatically resent to the user's email id after verifying his/her affiliations and requirements. This password is valid for 15 days. The user is allowed to download a sample dataset without registration to check if it fulfills the, before going for a complete download after registration.

4 Methodology

In this section, we have described the way PSO is used to enhance the contrast enhancement of an image. Figure 3 illustrates the flow of the study.

4.1 Transformation Function

A low contrast image reveals that it has low intensity value. A transformation function can be applied on a low contrast image to enhance the gray value of the image.

Let us consider a grayscale image with size $M \times N$ whose intensity value can be enhanced by a transformation function T based on both global and local enhancement methodology. The enhanced image matrix can be defined as:

$$x(i, j) = T[y(i, j)] \tag{2}$$

where $y(i, j)$ is the intensity value of the input image at position (i, j) and $x(i, j)$ is the intensity value of enhanced image at same position [14].

Local transformation function is applied on a user-defined window size $n \times n$ which can be defined as

$$x(i, j) = S(i, j)[y(i, j) - c \times p(i, j)] + p(i, j)^a \tag{3}$$

where n is the local mean and defined as

$$p(i, j) = \frac{1}{n \times n} \sum_{i=0}^{n-1} \sum_{j=0}^{n-1} y(i, j) \tag{4}$$

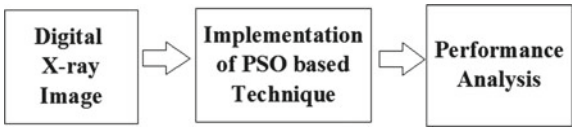

Fig. 3 Workflow

$K(i, j)$ is the enhancement function and defined as

$$S(i, j) = \frac{k.D}{\sigma(i, j) + b} \tag{5}$$

$\sigma(i, j)$ is the standard deviation of the window with size $n \times n$ and defined as

$$\sigma(i, j) = \sqrt{\frac{1}{n \times n}(\sum_{i=0}^{n}\sum_{j=0}^{n} y(i, j) - p(i, j)^2} \tag{6}$$

D is the global mean and defined as

$$R = \frac{1}{n \times n}\sum_{i=0}^{M-1}\sum_{j=0}^{N-1} y(i, j) \tag{7}$$

Finally, the transformation function is defined as

$$x(i, j) = \frac{k.R}{\sigma(i, j) + b}[y(i, j) - c \times p(i, j)] + p(i, j)^a \tag{8}$$

The value of the four parameters (a, b, c, k) are being optimized through parameter tuning are described in Sects. 4.2 and 4.3.

4.2 Objective Function

It is a measurement of quality of an image without any human intervention. While constructing the objective function, we have considered three properties of the enhanced images:

- A good contrast enhanced image has more number of edges than the original input image.
- An enhanced image has more intensity value than its edge.
- Entropy: This reveals the information content of an image. If the intensity distribution of the image is uniform, it should have high.

Hence, the objective function for this purpose is

$$F(I_e) = \log(\log E(I_s)) \times n_{edgles} \times H(I_e) \tag{9}$$

where I_e, I_s are the enhanced image and edge detected image, respectively. $E(I_s)$ is the sum of pixel intensity of edge detected image I_s. n_{edgles} is the number of edge pixels that have intensity value more than threshold value used in Sobel edge detector; in this case, we have used Otsu's global thresholding technique. Entropy of the image is calculated as

$$H(I_e) = -\sum_{i=0}^{255} e_i \tag{10}$$

$e_i = h_i \log_2 h_i$ if $h_i \neq 0$; otherwise, $e_i = 0$. h_i is the probability of a intensity value to be in the image. I_e is the enhanced image of an input image I.I_s is the edge image that can be defined using the kernel function described in Eqs. 12 and 13 and can be defined as

$$I_s = \sqrt{\delta m I_e(i, j)^2 + \delta n I_e(i, j)^2} \tag{11}$$

$$\delta m I_e = gI_e(i+1, j-1) + 2gI_e(i+1, j) + gI_e(i+1, j+1) - gI_e(i-1, j-1) - 2gI_e(i-1, j) - gI_e(i-1, j+1) \tag{12}$$

$$\delta n I_e = gI_e(i-1, j+1) + 2gI_e(i, j+1) + gI_e(i+1, j+1) - gI_e(i-1, j-1) - 2gI_e(i, j-1) - gI_e(i+1, j-1) \tag{13}$$

4.3 Particle Swarm Optimization

In this study, we have used PSO to obtain the optimal intensity value of the enhanced image. This technique is implemented based on the principle of swarm intelligence family. There are numerous techniques in swarm intelligence umbrella like genetic algorithm (GA), artificial bee colony (ABC), ant colony optimization (ACO), etc. GA computes the optimal solution using crossover and mutation. ACO and artificial bee colony (ABC) compute the optimal solution using food searching behavior of ant and bee swarm, respectively, whereas in PSO, it works based on the swarm behavior of bird [15]. In this study, we have used PSO to enhance the contrast of the image. The results clearly show that in case of X-ray image enhancement, PSO behaves better than the other members of swarm family. Each solution in this algorithm is known as particle. These particles are moved through the problem iteratively. Considering both local and global information of a low contrast image, the transformation function is used to enhance the gray value of the image using the objective functions. a, b, c, k are four parameters that are responsible to get the optimum result using fitness value, which is a parameter of good quality images. These values are computed through PSO mechanism. For a P number of particles, the four parameters are initialized within a range and equivalent to random velocities calculated as

$$v_i^{t+1} = w^t v_i^t + c_1 r_1 (pbest_i^t - X_i^t) + c_2 r_2 (gbest^t - X_i^t) \tag{14}$$

$$X_i^{t+1} = X_i^t + v_i^{t+1} \tag{15}$$

where X_i^t and v_i^t are the positions and velocity at time t, and W^t is the inertia weight which can be defined as

$$W^t = W_{max} \frac{W_{max} - W_{min}}{t_{max}} \times t. \tag{16}$$

Each vector for each particle has four components a, b, c, k. From this fitness value, the g_{best} and p_{best} known as local and global best values are calculated to direct the particle in a proper direction to obtain optimum solutions. Hence, new positions of particle lead to a better enhanced image of the histogram.

The contrast of the image is enhanced through the transformation function, which involves both global and local intensity values of the image. For each particle N, the four parameters represent the four components of the position vector. The parameter ranges defined in Sect. 4.3 represent the random velocity. This section described about the optimized velocity required in contrast enhancement. The quality of the image is measured through the objective function which is none other than the fitness of the particle. The *gbest* and *pbest* values help to move the particle toward the best position. In each iteration, a set of new particles have been generated along with its *gbest* and *pbest* values using the objective functions. The process is terminated when the image is enhanced through its *gbest* value.

4.3.1 Parameter Tuning

PSO is a parameter-dependent algorithm. Gray value enhancement of benchmark image using PSO is introduced in [14], and they have used the value of four parameters used in this PSO-based enhancement method which lies between $a \in [0, 1.5]$, $b \in [0, 0.5]$, $c \in [0, 1]$, $k \in [0.5, 1.5]$.

However, there are some differences in properties of normal images with those of the medical images. All the images generated from same X-ray scanner machine have the same intensity property. Hence, to calculate the optimal value of each parameters, we have executed Algorithm 1, which yields the fitness value described in Eq. 9 in a range of $a \in [0, 2]$, $b \in [0, 1.2]$, $c \in [0, 2]$, $k \in [0, 2]$. The value of b changes the output image drastically and is extremely sensitive. Figure 6 clearly shows that with very high and very low value of the above-mentioned parameter b generates a binary image. The plots shown in Fig. 4a, b, c are three-dimensional line plots, where fitness value is plotted against any two variables keeping the third variable constant. These three plots yield a pair of value for each of the variables. Finally, the optimum values for the variables are calculated by averaging it.

Algorithm 1 PSO in Contrast Enhancement

Input: Low Contrast Image
Output: Contrast Enhanced Image

1: Define N number of particles with m dimension
2: values of parameter a,b,c,k are initialized
3: **for** Each Particle $i = 1$ to N **do**
4: gbest and pbest of each particles are calculated using Equation 9.
5: The inertia weight (W) is calculated as

$$W^t = W_{max} - \frac{W_{max} - W_{min}}{t_m ax} \times t. \tag{17}$$

6: **while** (gbest$\neq$ pbest)& $W^t > W_{min}$ **do**
7: Calculate fitness value using the objective function described in 9
8: **if** $T(I_e)_i < T(pbest_i)$ **then**
9: $pbest_i = N_i$
10: **end if**
11: **if** $T(I_e)_i > T(gbest_i)$ **then**
12: $gbest_i = N_i$
13: **end if**
14: Update velocity and position using Equation 14 and 15
15:
16: Enhanced Image is generated using Equation 8
17: **end while**
18: **end for**

Figure 4a shows that value of (a, k) is (0.7, 0.9)
Figure 4b shows that value of (k, c) is (0.7, 0.8)
Figure 4c shows that value of (a, c) is (0.9, 0.9)

Hence, $a = 0.8$, $k = 0.85$, $c = 0.9$. The window size is determined according to the base exposure of the image. Higher the window size, the enhanced image will be more smoother, i.e., more articulation will be there in the output image. Lesser the window size, the output image produced will be toward a binary image, and is used in case of moderate exposure images. The window size needs to be optimized to enhance any presence of any abnormal entity. However, in case of any low exposure image, the window size needs to be large, to enhance the image and to provide more accurate estimation of any presence of any external entity and also to provide a better fitness value of the enhanced image. Figure 5 shows that at $n \leq 30$ and $n \geq 50$ yields a binary image.

Fig. 4 3D Plot for parameter tuning

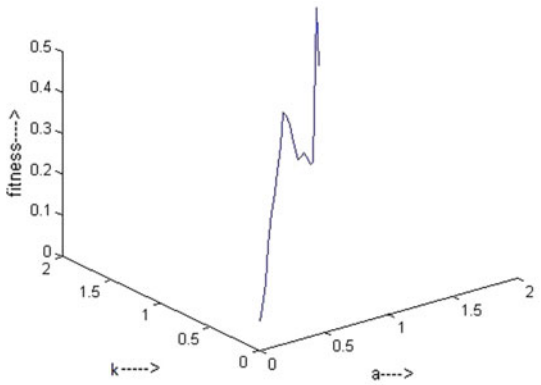

(a) variation of Fitness function with respect to a,k

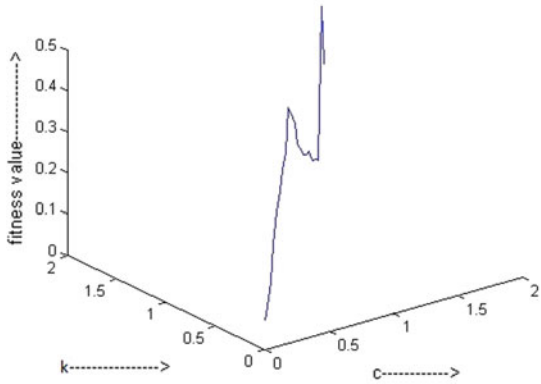

(b) variation of Fitness function with respect to k,c

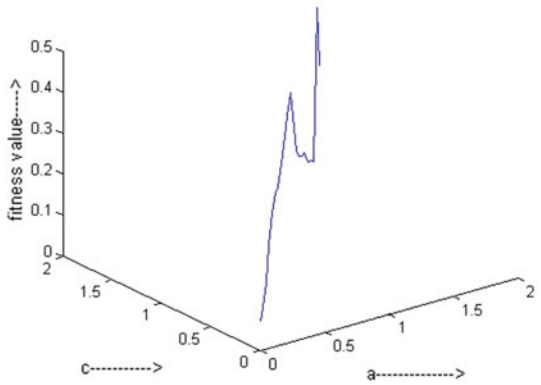

(c) variation of Fitness function with respect to a,c

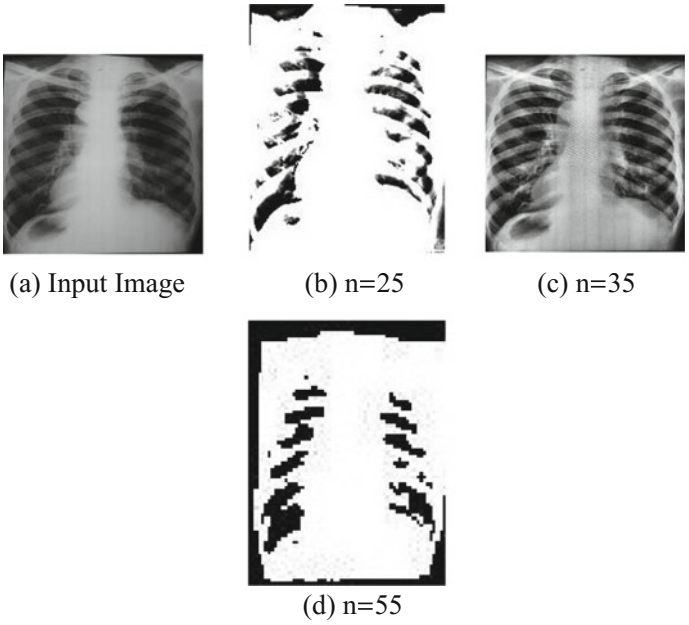

Fig. 5 Output based on window size

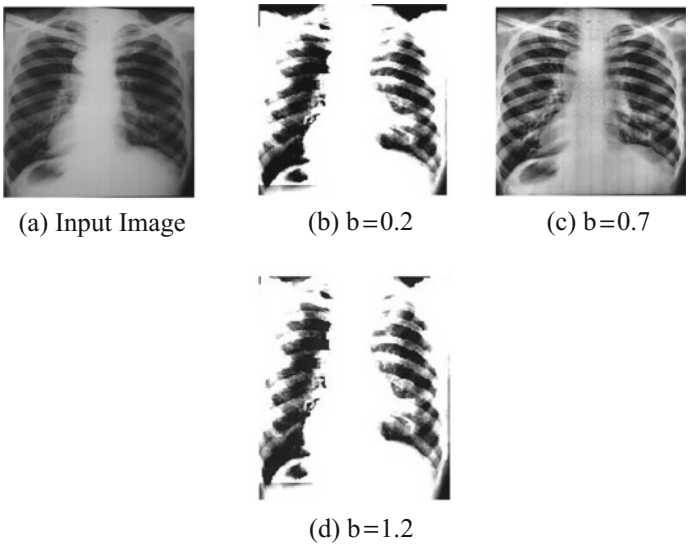

Fig. 6 Result of parameter tuning for variable b

5 Results and Discussion

In this section, we display the result of our contrast enhancement algorithm over digital X-ray images. To establish the performance of PSO-based contrast enhancement algorithm, we have analyzed the performance of PSO over some standard contrast enhancement techniques like histogram equalization (HE) [16], linear contrast stretching (LCS), adaptive histogram equalization (AHE) [7], adjustment function [16], median-mean-based sub-image-clipped histogram equalization (MNSICHE) [9], BPFDHE [11], nonparametric modified histogram equalization (NHMC) [8] using some standard metric described in Sect. 5.3. We have executed our algorithm over all images of the dataset, however results of 5 randomly chosen images are shown below among them, Image ID 1–3 are high contrast and 4 and 5 are low contrast images.

5.1 Dataset

We have used 220 chest X-ray images collected from Peerless Hospital from March 2015 to March 2017 for those patients who came for their routine check up with different types of lung diseases for contrast enhancement [17]. The patient edge lies between 30–75 which consists of both male and female patients. Among 220 patients, 157 patients are male and rest are female. In conventional X-ray imaging procedure, the X-ray beam passes through the human body the shadow of hard tissue as shadow on the film. This film is then processed and printed to get the picture of the organ. In this study, we have used CR type of digital X-ray images where a sensor is placed behind the patient instead of placing X-ray films in conventional radiography. This sensor is next attached to the computer to create the digital radiography [18].

5.2 Result of Annotation Process

Three experienced radiologist have been found 300 abnormalities from 120 chest radiographs, among them, 257 cases are marked as nodule by at least one radiologists and 227 cases marked as nodule by all radiologists. Although, Biopsy and cytology report says that there present 252 nodules and among them 193 cases are malignant rest are benign among all the malignant cases 70 are responsible for metastatic lung cancer.

The type of nodule is further categorized into five classes, namely obvious, relatively obvious, subtle, very subtle, and extremely subtle. There are 86 nodules that are very subtle, 31 nodules are extremely subtle, 48 nodules are subtle, 64 nodules are obvious, and the rest of 33 nodules are relatively obvious.

Anatomy of human lung reveals that there are five lobes and generation in different positions has different chances of malignancy. There are 88 nodules that are in left lower lobe, 72 nodules are in left upper lobe, 10 nodules are in the right middle lobe, 56 nodules are in right lower lobe, and 26 nodules are in right upper lobe.

5.3 Evaluation Metrics

- Peak signal-to-noise ratio(PSNR): PSNR can be defined as the ratio between the maximum power of the signal and the power of the corrupting noise, which measures the peak error. Higher the PSNR value indicates the higher quality of images. Mathematically, $PSNR$ can be defined as:

$$PSNR = 20\log_{10}\left(\frac{255}{RMSE}\right) \tag{18}$$

- Mean square error:

$$MSE = \sqrt{\frac{1}{n}\sum_{i=1}^{n}(x-y)^2} \tag{19}$$

  where x is the output image and y is the reference image.
- Mean absolute brightness error (MABE): It is the measurement of absolute intensity value difference between input image and enhanced image

$$D = \|\mu_A - \mu_B\|. \tag{20}$$

  An algorithm generating less value is considered as good one.
- Detailed variance:
- Background variance:

Figure 7 exhibits the visual verification result of input chest X-ray images. The input image in Fig. 7 is much lower in contrast than that of the input images of Fig. 8. The output of these figures along with their histogram clearly shows that PSO works better in case of comparatively very low contrast X-ray images even it suppresses the ribs which are not our region of interest. However in comparatively high contrast images, it does not score very high. Tables 2, 4, 1 clearly show that PSO-based image enhancement algorithm works better than the modified histogram equalization methods. However, the visual verification result always does not give the guarantee of perfect results (Figs. 9 and 10).

According to the definitions of fitness value, PSNR, Detailed Variance, Background Variance and MABE, MSE a good contrast image has higher fitness value, PSNR, detailed variance and background variance and least value in case of MABE and MSE. The comparative analysis of this metric is described in Tables 1, 2, 3, 4, 5, 6 and Figs. 9, 8, 11, 12, 13, 14.

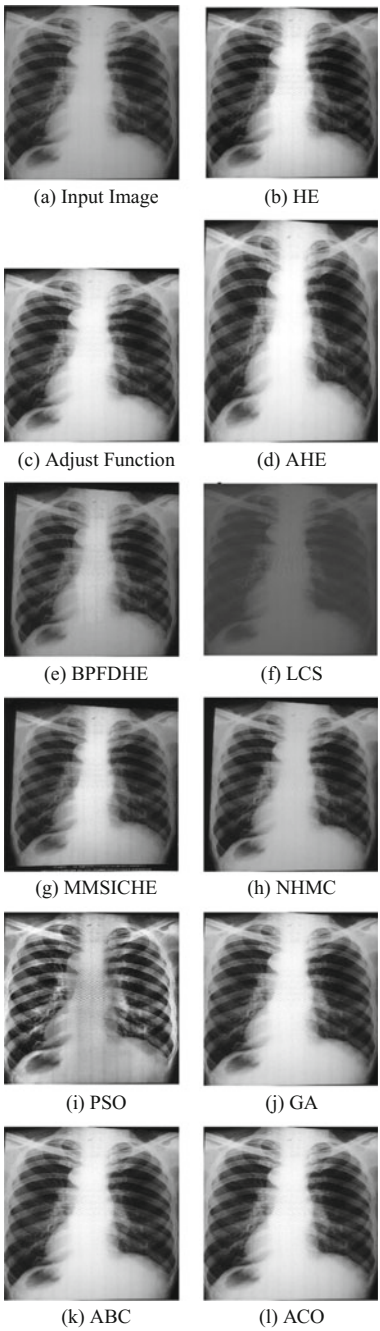

Fig. 7 Visual verification of PSO over other algorithm for low contrast image

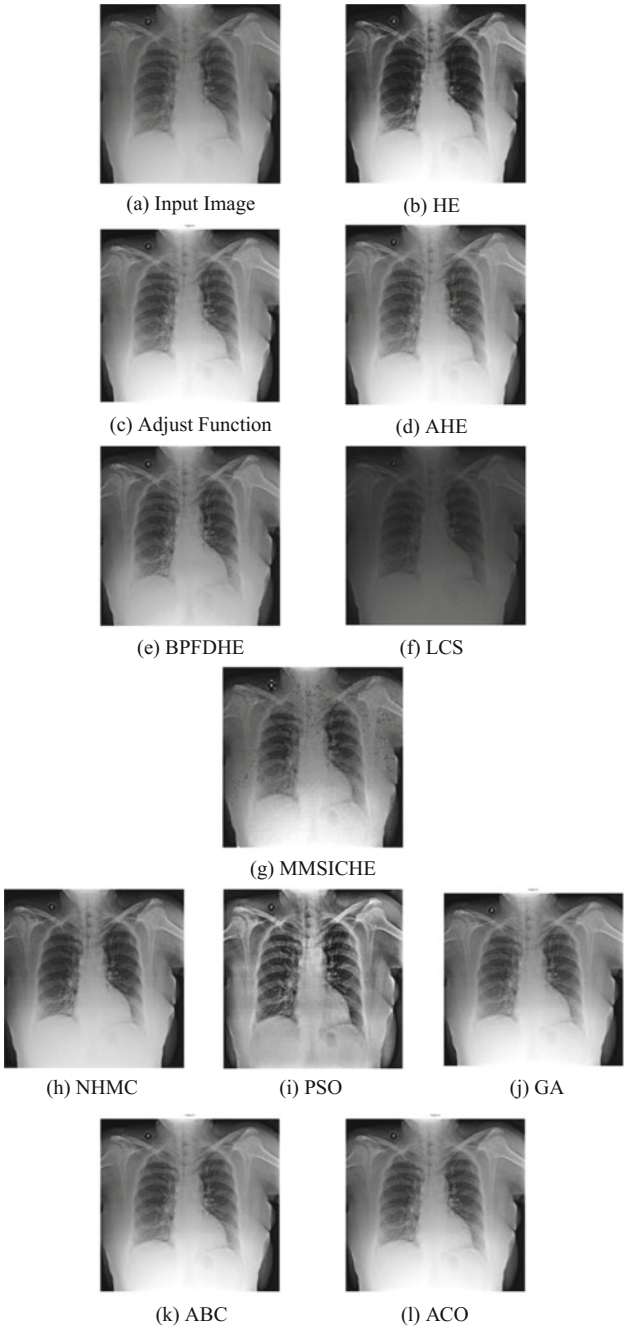

Fig. 8 Visual verification of PSO over other algorithm for high contrast images

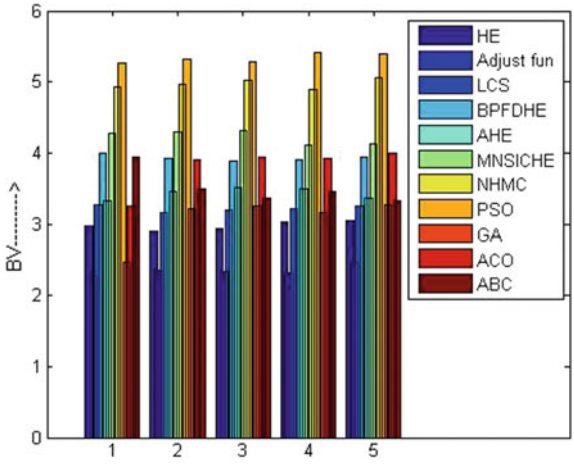

Fig. 9 Background variance

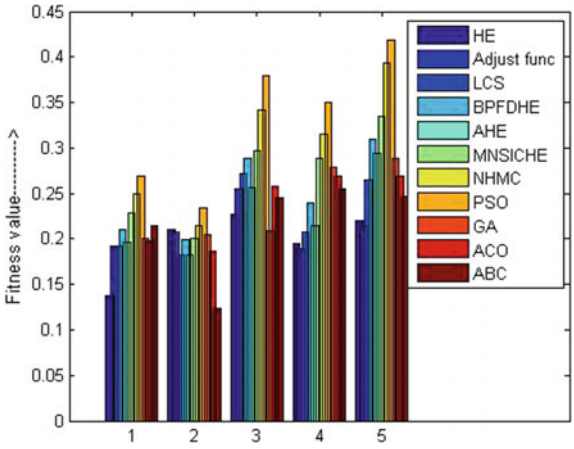

Fig. 10 Comparison of fitness value

Table 1 Fitness function value of different algorithms

Image	HE	Adjust	LCS	BPFDHE	AHE	MNSICHE	NHMC	PSO	GA	ACO	ABC
ID1	0.138	0.192	0.192	0.210	0.197	0.229	0.250	0.269	0.201	0.198	0.215
ID2	0.210	0.208	0.182	0.199	0.182	0.201	0.214	0.234	0.205	0.187	0.123
ID3	0.227	0.255	0.272	0.289	0.257	0.297	0.342	0.379	0.209	0.258	0.245
ID4	0.195	0.189	0.207	0.239	0.214	0.288	0.315	0.350	0.279	0.269	0.255
ID5	0.220	0.215	0.265	0.310	0.294	0.3347	0.393	0.419	0.289	0.269	0.247

Table 2 Comparison of background variance

Image	HE	Adjust	LCS	BPFDHE	AHE	MNSICHE	NHMC	PSO	GA	ACO	ABC
ID1	2.97	2.28	3.27	3.99	3.32	4.27	4.92	5.27	2.46	3.25	3.94
ID2	2.89	2.36	3.15	3.92	3.45	4.29	4.96	5.32	3.21	3.91	3.49
ID3	2.94	2.34	3.19	3.89	3.52	4.31	5.02	5.29	3.25	3.94	3.37
ID4	3.02	2.32	3.21	3.91	3.49	4.11	4.89	5.41	3.15	3.92	3.45
ID5	3.05	2.46	3.25	3.94	3.37	4.13	5.06	5.39	3.27	3.99	3.32

Table 3 Detailed variance generated by different algorithms

Image	HE	Adjust	LCS	BPDHE	AHE	MNSICHE	NHMC	PSO	GA	ACO	ABC
ID1	0.1873	0.1507	0.2030	0.2870	0.2507	0.3005	0.3220	0.3350	0.2356	0.2545	0.2356
ID2	0.1806	0.1512	0.2005	0.2805	0.2520	0.2997	0.3216	0.3370	0.1245	0.1986	0.2109
ID3	0.1897	0.1577	0.2078	0.2890	0.2594	0.3047	0.3205	0.3397	0.2589	0.2548	0.2989
ID4	0.1809	0.1502	0.2009	0.2820	0.2509	0.3020	0.3195	0.3398	0.2256	0.2548	0.2378
ID5	0.1825	0.1508	0.2083	0.2837	0.2610	0.3017	0.3189	0.3390	0.2356	0.2454	0.2545

Table 4 Mean absolute brightness error

Image	HE	Adjust	LCS	BPFDHE	AHE	MNSICHE	NHMC	PSO	GA	ACO	ABC
ID1	22.17	27.33	24.67	16.23	20.13	15.51	12.72	9.44	10.23	11.89	12.56
ID2	22.52	27.45	23.78	15.52	19.89	1.23	13.23	10.15	10.02	11.89	12.56
ID3	22.12	28.06	23.52	16.09	20.05	15.21	12.99	9.74	12.23	11.56	12.89
ID4	21.86	27.96	24.26	15.89	19.97	15.04	12.85	9.56	13.26	15.30	11.56
ID5	22.05	27.69	23.56	15.75	19.56	15.53	12.89	9.45	13.02	12.56	15.23

Table 5 Peak signal-to-noise ratio

Image	HE	Adjust	LCS	BPFDHE	AHE	MNSICHE	NHMC	PSO	GA	ACO	ABC
ID1	42.17	47.33	54.67	46.23	50.13	45.51	42.72	59.14	54.12	55.45	57.89
ID2	42.52	47.45	53.78	45.52	49.89	4.23	43.23	60.25	53.93	55.01	56.89
ID3	42.12	48.06	53.52	46.09	50.05	45.21	42.99	63.74	54.21	54.69	56.05
ID4	41.86	47.96	54.26	45.89	49.97	45.04	42.85	62.56	54.01	55.23	57.09
ID5	42.05	47.69	53.56	45.75	49.56	45.53	42.89	59.45	53.22	54.95	57.22

Table 6 Mean square error

Image	HE	Adjust	LCS	BPFDHE	AHE	MNSICHE	NHMC	PSO	GA	ACO	ABC
ID1	61.23	65.12	60.23	66.23	55.13	41.51	42.72	19.14	54.12	25.45	37.89
ID2	62.78	65.45	60.56	65.52	55.89	41.23	43.23	19.25	53.93	25.01	36.89
ID3	61.95	65.89	60.45	66.09	56.05	42.21	42.99	20.74	54.21	24.69	36.05
ID4	62.12	64.89	60.78	65.89	56.97	43.04	42.85	19.56	54.01	25.23	37.09
ID5	63.12	67.23	60.12	65.75	56.56	42.53	42.89	19.45	23.22	54.95	37.22

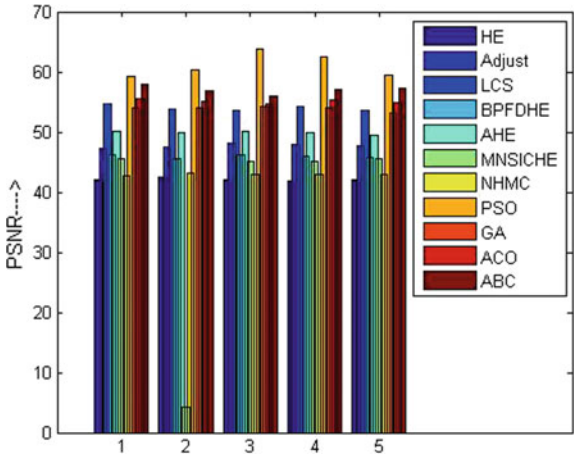

Fig. 11 Comparison of PSNR

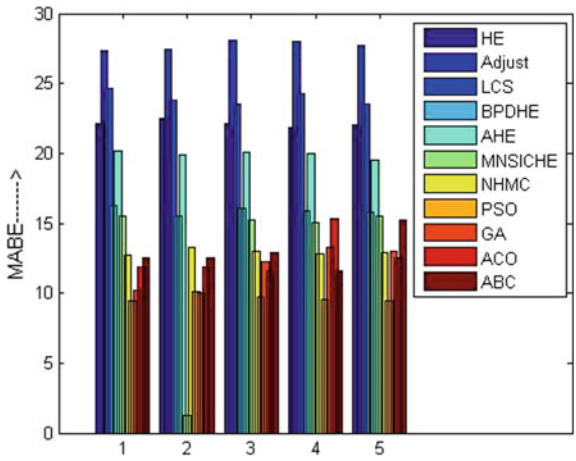

Fig. 12 Comparison of entropy

Table 7 Result of cross-validation

ID	FitnessValue	BV	DV	PSNR	MSE	MABE
Image1	0.269	5.27	0.3350	98.56	0	0
Image2	0.234	5.32	0.3370	98.78	0	0
Image3	0.379	5.29	0.3397	98.95	0	0
Image4	0.350	5.41	0.3398	99.23	0	0
Image5	0.419	5.39	0.3390	99.04	0	0

To ensure that the output enhanced images are optimized, we have passed the output image as input image in algorithm to calculate difference metrics as described in Sect. 5.3. The evaluated metric values are shown in Table 7.

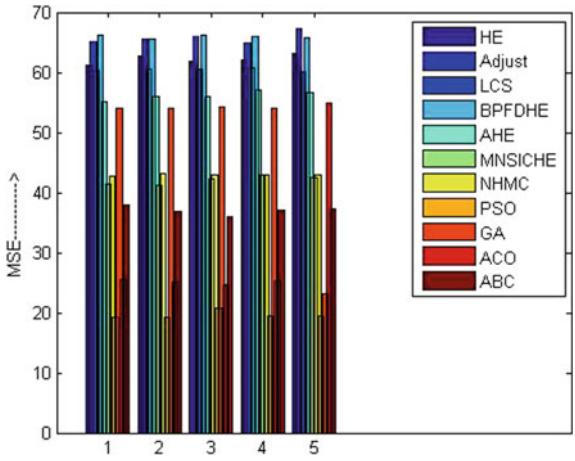

Fig. 13 Comparison of mean square error

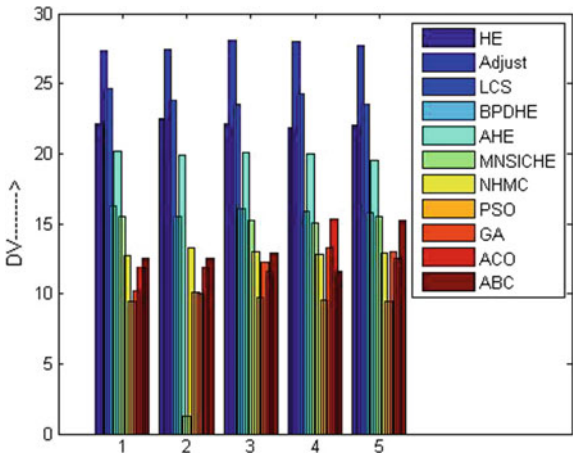

Fig. 14 Comparison of detailed variance

6 Conclusion

Contrast enhancement of medical images is quite a challenging task in medical image analysis. In this paper, we have applied particle swarm optimization over digital X-ray images. The results in comparison with the other existing techniques are quite satisfactory. In future, we will apply more accurate objective function and/or any other bio-inspired meta-heuristic techniques rather than swarm intelligence to get better enhanced images.

7 Conflict of Interest and Ethical Issues

The authors declare that they have no conflict of interest.

The collection of patient scans images and pathological report for research purpose was approved by the Ethical Committee of Peerless Hospital and B. K. Roy Research Centre Ltd, Kolkata on January 30, 2015 with reference number: PH&BKRRCCREC/1576/2015. This study is approved till January 2020. However, the issue of publishing the collected patient images as a public dataset was approved by the same ethical committee dated on August 4, 2016, with reference number:PH&BKRRCCREC/2063/2016, abide by all the ethical guidelines of a retrospective study generated by the Indian Council of Medical Research (ICMR).

Acknowledgements We are thankful to Center of Excellence in Systems Biology and Biomedical Engineering (TEQIP II) of University of Calcutta for providing the financial support for this research and Peerless Hospitex Hospital for providing their valuable image dataset.

References

1. International Agency for Cancer Research Globocan 2012 Estimated Cancer Incidence, mortality and Prevalence Worldwide in 2012
2. Heath, M., Bowyer, K., Kopans, D., Moore, R., Kegelmeyer Jr P.: The digital database for screening mammography, vol. 58, pp. 27,96
3. Shiraishi, Junji, Katsuragawa, Shigehiko, Ikezoe, Junpei, Matsumoto, Tsuneo, Kobayashi, Takeshi, Komatsu, Ken-ichi, Matsui, Mitate, Fujita, Hiroshi, Kodera, Yoshie, Doi, Kunio: Development of a digital image database for chest radiographs with and without a lung nodule: receiver operating characteristic analysis of radiologists' detection of pulmonary nodules. Am. J. Roentgenol. **174**(1), 71–74 (2000)
4. Sherrier, R.H., Johnson, G.A.: Regionally adaptive histogram equalization of the chest. IEEE Trans. Med. Imaging, **6**(1), 1–7 (1987)
5. Altas, Irfan, Louis, John, Belward, John: A variational approach to the radiometric enhancement of digital imagery. IEEE Trans. Image Process. **4**(6), 845–849 (1995)
6. Chen, S.D., Ramli, A.R.: Contrast enhancement using recursive mean-separate histogram equalization for scalable brightness preservation. IEEE Trans. Consum. Electron. **49**(4), 1301–1309 (2003)
7. Zuiderveld, K.: Contrast limited adaptive histogram equalization, Graphics gems IV, pp. 474–485. Academic Press Professional, Inc (1994)
8. Poddar, S., Tewary, S., Sharma, D., Karar, V., Ghosh, A., Pal, S.K.: Non-parametric modified histogram equalisation for contrast enhancement. IET Image Process. **7**(7), 641–652 (2013)
9. Singh, Kuldeep, Kapoor, Rajiv: Image enhancement via median-mean based sub-image-clipped histogram equalization. Opt. Int. J. Light Electron Opt. **125**(17), 4646–4951 (2014)
10. Xue, Q.: Enhancement of medical images in the shearlet domain. In: Computer Science and Network Technology (ICCSNT), 2013 3rd International Conference on, pp. 235–238. IEEE (2013) (October)
11. Sheet, Debdoot, Garud, Hrushikesh, Suveer, Amit, Mahadevappa, Manjunatha, Chatterjee, Jyotirmoy: Brightness preserving dynamic fuzzy histogram equalization. IEEE Trans. Consum. Electron. **56**(4), 2475–2481 (2010)
12. Yang, H.Y., Lee, Y.C., Fan, Y.C., Taso, H.W.: A novel algorithm of local contrast enhancement for medical image. In: Nuclear Science Symposium Conference Record, 2007. NSS'07, vol. 5, pp. 3951-3954. IEEE (2007) (October)

13. Hashemi, S., Kiani, S., Noroozi, N., Moghaddam, M.E.: An image contrast enhancement method based on genetic algorithm. Pattern Recognit. Lett. **31**(13), 1816–1824 (2010)
14. Gorai, A., Ghosh, A.: Gray-level image enhancement by particle swarm optimization. In: World Congress on Nature & Biologically Inspired Computing, 2009. NaBIC 2009, pp. 72–77 (2009)
15. Eberhart, R.C., Kennedy, J.: A new optimizer using particle swarm theory. In: Proceedings of the Sixth International Symposium on Micro Machine and Human Science, vol. 1, pp. 39–43 (1995)
16. Gonzalez, R.C., Woods, R.E.: Digital image processing, 3rd edn. Tata MacgrawHill (2008)
17. http://www.coe.cuteqip.net/coepeerlessxray.php
18. Wendt, R.: The Mathematics of Medical Imaging: A Beginner's Guide, pp. 1987–1987 (2010)
19. Stetson, P.F., Sommer, F.G., Macovski, A.: Lesion contrast enhancement in medical ultrasound imaging. IEEE Trans. Med. Imaging **16**(4), 416–425 (1997)
20. Zhu, H., Chan, F.H., Lam, F.K.: Image contrast enhancement by constrained local histogram equalization. Comput. Vis. Image Underst. **73**(2), 281–290 (1999)
21. Al-Manea, A., El-Zaart, A.: Contrast enhancement of MRI images. In: Ibrahim, F., Osman, N.A.A., Usman, J., Kadri, N.A. (eds) 3rd Kuala Lumpur International Conference on Biomedical Engineering 2006. IFMBE Proceedings, vol 15. Springer, Berlin, Heidelberg (2007)
22. Knopp, M.V., Giesel, F.L., Marcos, H., von Tengg-Kobligk, H., Choyke, P.: Dynamic contrast-enhanced magnetic resonance imaging in oncology. Top. Magn. Reson. Imaging **12**(4), 301–308 (2001)